

PRISM L2 and L3 Algorithm Theoretical Basis and Preliminary Validation

David R. Thompson^a, Michelle Gierach^a, Heidi Dierssen^b, Robert O. Green^a,
Justin Haag^a, Sarah Lundeen^a, Ian McCubbin^a, Pantazis Mouroulis^a

^a*Jet Propulsion Laboratory, California Institute of Technology, Pasadena CA 91109, USA*

^b*University of Connecticut*

1. Reflectance Retrieval

The PRISM *Level 2* atmospheric correction algorithm removes the effects of atmospheric absorption and scattering to estimate the water-leaving reflectance, r_s , directly above the water surface. This quantity is equivalent to the Hemispherical Directional Reflectance Function, or HRDF (Schaepman-Strub et al., 2006), which is related to the commonly-used Remote Sensing Reflectance R_{rs} by $r_s = \pi R_{rs}$. This retrieval uses a modified version of the ATmospheric RE-Moval (ATREM) approach by Gao et al. (Gao & Goetz, 1990; Gao et al., 1993) with further adjustments to the solar irradiance model detailed in Thompson et al. (2015b). This section describes the L2 algorithm and our validation procedure. The algorithm begins with a spectral image of calibrated radiances at each known wavelength channel, and we assume all relevant *Level 1* radiometric and spectral analyses have already been applied.

We first normalize these radiances for variable solar illumination, transforming them into a *top of atmosphere reflectance* spectrum ρ by accounting for the solar irradiance F , and solar incidence angle ψ :

$$\rho = \frac{\pi L}{F \cos(\psi)} \quad (1)$$

As detailed in Gao et al. (1993), neglecting the coupling between absorption and scattering, ρ is approximately related to the apparent surface r_s by:

$$r_s = \frac{\rho/T_g - r_a}{T_d T_u + s(\rho/T_g - r_a)} \quad (2)$$

where T_g is the gaseous transmission of the atmosphere, T_u and T_d are upward and downward transmission due to scattering, s is the spherical sky albedo and r_a is the path reflectance due to scattering effects. Scattering terms combine molecular (Rayleigh) scattering as well as particle scattering due to aerosols. We calculate these coefficients in advance using the 6s code (Vermote et al., 1997; Teillet, 1989; Tanré et al., 1990) based on a model atmosphere. For retrievals

over land, elevation can be variable so the pressure elevation of the scene is not known in advance and must be retrieved at runtime. In those cases, we calculate coefficients for 5 candidate elevations spaced at regular intervals from sea level to 4 kilometers, or up to the altitude of the aircraft, as in Thompson et al. (2015a).

We calculate reference transmissions using gas absorption coefficients derived from the Oxford Reference Forward Model (Dudhia, 2014) using the HITRAN 2012 line list (Rothman et al., 2013) and transform them to the instrument spectral resolution by convolution with the PRISM instrument response function. We model transmission of all significant gases including H₂O, O₂, CO₂, CH₄, CO and N₂O. The gas absorption coefficients also depend on pressure elevation, as well as the spatially-variable concentration of H₂O vapor. Consequently we calculate gas transmission values and aerosol coefficients for 60 candidate water vapor abundances spaced logarithmically from a column water vapor concentration of 0 to 5cm.

At these initial calculations, all the coefficient values needed for calculation of Equation 2 (independently for each wavelength) are been stored in a 2-dimensional lookup table parameterized by the H₂O vapor absorption path and by pressure altitude. At runtime, we retrieve the atmospheric state using characteristics of each TOA spectrum, and then look up the precise coefficients using bilinear interpolation. For land surfaces, we estimate pressure altitude using a Continuum Interpolated Band Ratio (Bruegge et al., 1990; ?) of the 760nm Oxygen A band, provided by the following expression where ρ_m , ρ_l and ρ_r represent TOA values in the middle, left and right edges of the band, and ω are weighting factors that equalize the contribution of each side:

$$R_{CIBR} = \rho_m / (\omega_r \rho_r + \omega_l \rho_l) \quad (3)$$

Similarly, we find the H₂O vapor path using a CIBR estimate of 820nm or 940nm absorption features. A linearized nonnegative spectrum fit refines this estimate as per Thompson et al. (2015a). After retrieving water vapor and pressure altitudes, we apply the reflectance calculation of Equation 2. For open-water spectra, it is not always possible to observe the oxygen A band due to low signal levels at 760 nm over water. In these flightlines, we set the pressure elevation to sea level.

Special care is needed when modeling the solar irradiance spectrum. The solar spectrum in blue and UV wavelengths varies slightly over time, and the fine solar absorption lines in this region make the measurement highly sensitive to the instrument response function. We account for these challenges by optimizing the solar irradiance spectrum following the procedure in Thompson et al. (2015b). This process minimizes residual features based on a known spectrally-smooth reference target, adjusting the canonical irradiance spectrum as detailed in that article and posted on the PRISM web site (PRISM, 2015).

Finally, we perform a cosmetic smoothing using multiplicative coefficients for each channel to reduce atmospheric residuals and other systematic bumps in the reflectance spectra. These coefficients are derived from a spectrally-smooth

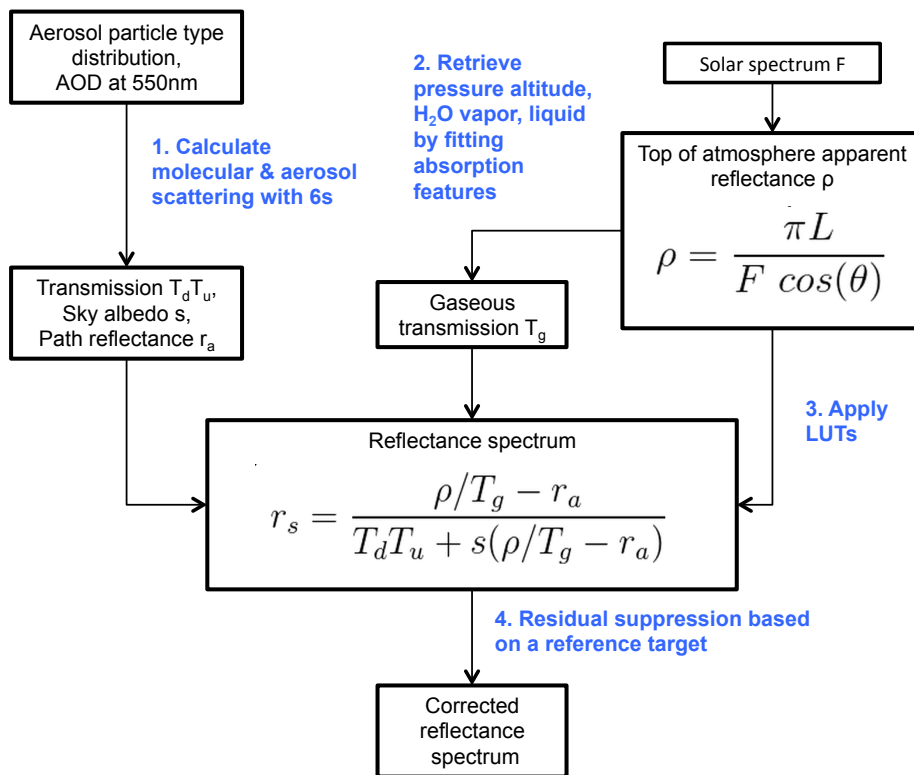


Figure 1: Atmospheric correction procedure.

feature or in-situ reference target; we match the spectrum to the known, smooth reflectance from the ground measurement. We retain only high-frequency components of this correction, holding the overall magnitude close to unity. Figure 1 shows the complete procedure.

We validated these reflectance retrievals by overflying large targets for which ground-truth properties are known from in-situ measurements. We applied PRISM radiometric and reflectance analysis to canonical test scenes such as Ivanpah playa, NV Green et al. (1998). Figure 1 shows a direct comparison between an in-situ reflectance measurement acquired by an Analytical Spectral Devices field spectrometer (ASD), and the remote reflectance estimate (PRISM), over the bright playa surface. The remote spectrum was produced by inverting an airborne observation by a high-altitude ER-2 aircraft overflying the site in autumn 2015. The close match suggests that radiometric and spectral calibrations are accurate, and that atmospheric correction calculations model these conditions to accuracies of approximately 1-3% over the relevant spectral ranges.

Ivanpah playa, remote and in situ

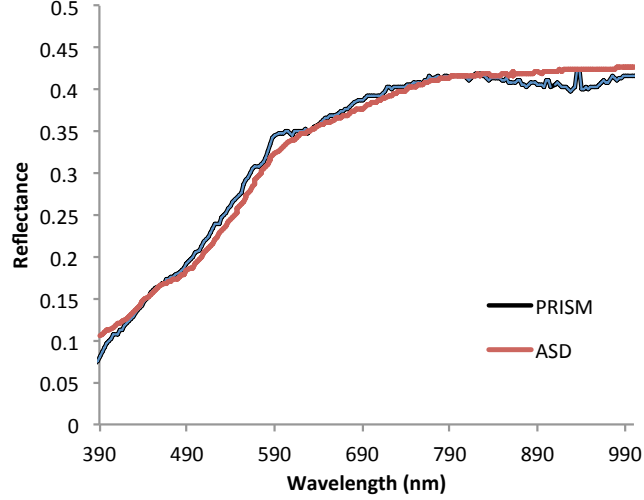


Figure 2: Exemplar spectra from Ivanpah Playa, NV

2. Water property retrieval

The PRISM analysis chain offers two alternative versions of the Chlorophyll retrieval: a *quick look*, and a *spectroscopic* analysis. The *quick look* is based on existing multiband retrieval algorithms for instruments such as MODIS and SeaWiFS. It permits a fast assessment of phytoplankton populations, suitable for use in the field or for direct comparisons with these other datasets. The file consists of four bands containing different multiband estimates of Chlorophyll-a, each of which makes slightly different assumptions about the populations and water properties. The four are summarized and validated in Johnson et al. (2013). They include the standard SeaWiFS OC4v6 approach (O’Reilly et al., 2000),

$$Chl_{SW} = 10^{0.3272 - 2.994R_{SW} + 2.7218R_{SW}^2 - 1.2258R_{SW}^3 - 0.5683R_{SW}^4} \quad (4)$$

where R_{SW} represents the base-10 logarithm of the maximum of the three ratios $R_{rs}(443)/R_{rs}(555)$, $R_{rs}(490)/R_{rs}(555)$, and $R_{rs}(510)/R_{rs}(555)$. The second channel is the MODIS-Aqua OC3M formula (?).

$$Chl_{MA} = 10^{0.2424 - 2.7423R_{SW} + 1.80178R_{SW}^2 - 0.0015R_{SW}^3 - 1.228R_{SW}^4} \quad (5)$$

where R_{MA} represents the base-10 logarithm of the maximum of the two ratios $R_{rs}(443)/R_{rs}(555)$, and $R_{rs}(490)/R_{rs}(555)$.

Note that the values Chl_{SW} and Chl_{MA} are likely to underestimate Chlorophyll-a in the Southern Ocean due to its distinct bio-optical properties. Consequently,

we also offer revised estimates based on the empirical formula of Johnson et al. (2013). The Southern Ocean version of the SeaWiFS algorithm is:

$$Chl_{SSW} = 10^{0.6736 - 2.0714R_{SW} + 0.4939R_{SW}^2 - 0.4756R_{SW}^3} \quad (6)$$

The Southern Ocean version of MODIS-Aqua is:

$$Chl_{SMA} = 10^{0.6994 - 2.0384R_{MA} + 0.4656R_{MA}^2 - 0.4337R_{MA}^3} \quad (7)$$

No PRISM data for the Southern Ocean was available prior to deployment, so we validated these methods using in-situ measurements of Chlorophyll-a that acquired on the Palmer LTER array Moline et al. (1997) coincident with orbital observations by the MERIS, MODIS-Aqua, and SeaWiFS instruments. The *in situ* collections and remote acquisitions took place on the same day for each of 31 separate cloud-free instances in January over the span from 2003-2010. We extracted the pixel of the appropriate water-leaving reflectance product for each instrument, and performed the MODIS OC3M retrievals using the standard algorithm (yielding Chl_{MA}) and the Johnson et al. (2013) Southern Ocean revision (yielding Chl_{SMA}). Figure 2 shows the matches and correlations for each sensor and retrieval algorithm. The MODIS OC3 methodology and variant is used. The Southern Ocean adjustments consistently bring the results closer to the in situ measurement, further corroborating the Johnson et al. (2013) study. The lower-right plot shows a comparison of the MODIS and MERIS image retrievals, indicating the degree of natural divergence that would be expected due to distinct spatial sampling and temporal variability during the day.

For a longer and more complete analysis, we also provide a full *spectroscopic* retrieval of water properties using the deep water model of (Lee et al., 2004). We first correct for the effects of the water/air interface, transforming the remote sensing reflectance R_{rs} into the remote sensing reflectance below the water surface, written r_{rs} . We use the following empirical relation, derived from (Lee et al., 1998) Equation 25:

$$r_{rs} = \frac{R_{rs} - Q}{1.562(R_{rs} - Q) + 0.518} \quad (8)$$

where Q is a spectrally-constant parameter derived during the retrieval, related to the smooth spectral reflectance of surface glint. For deep waters, we can then relate the remotely-sensed reflectance below the water interface to optical properties of absorption a and backscatter b_b using:

$$r_{rs} = g_w \frac{b_{bw}}{a + b_b} + g_p \frac{b_{bp}}{a + b_b} \quad (9)$$

where g_w and g_p are coefficients for the backscatter due to water, b_{bw} , and particulates, b_{bp} , respectively. The total backscatter is the simple sum of the two backscatter components, $b_b = b_{bw} + b_{bp}$. The g_w and g_p coefficients are dependent on the solar incidence angle and observation geometry, and are derived empirically using radiative transfer models in Lee et al. (2004). That

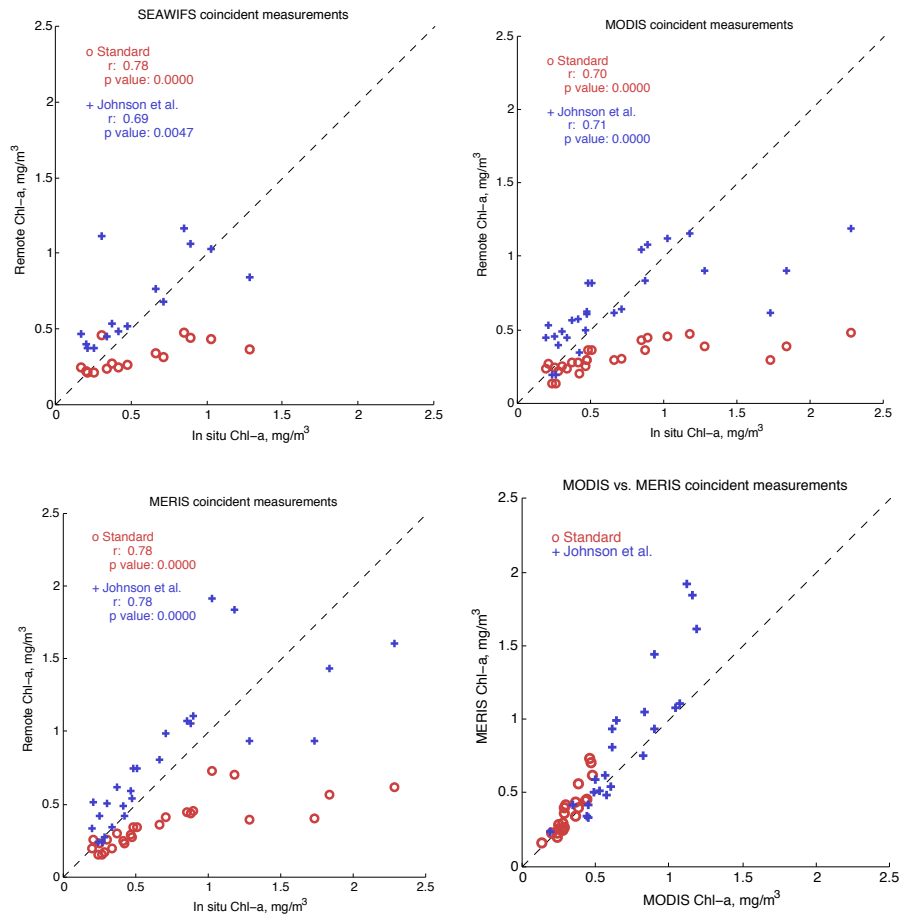


Figure 3: Comparison of in-situ Chl-a measurements and remote Chl-a retrievals using the quicklook algorithms.

work presents both a nadir-viewing and an off-nadir option. We find the result is fairly insensitive to this choice, but that the off-nadir coefficients provide slightly better performance. There, g_w is held fixed at 0.111, and the coefficient g_p is defined as:

$$g_p = G_0 \left(1.0 - G_1 e^{-G_2 \frac{b_{bp}}{a+b_b}} \right) \quad (10)$$

Where $G_0 = 0.189$, $G_1 = 0.627$, and $G_2 = 3.204$. The backscatter due to water is well established (Morel, 1974), while the particle backscatter is defined for each wavelength λ as in Lee et al. (1998), using an intermediate quantity Y held to the $[0, 2.5]$ interval, and another quantity X that is retrieved as a free parameter:

$$b_{bp} = X \left(\frac{400.0}{\lambda} \right)^Y \quad (11)$$

$$Y = 3.44(1 - 3.17e^{2.01\chi}), \quad 0 \leq Y \leq 2.5 \quad (12)$$

$$\chi = R_{rs}(440)/R_{rs}(490) \quad (13)$$

Finally, we calculate absorption as the sum of absorption coefficients by water, a_w , phytoplankton, a_ϕ , and detritus a_g , using the following formula:

$$a = a_w + a_\phi + a_g a_g = G e^{-0.015(\lambda-440)} \quad (14)$$

$$a_\phi = \Phi_1 P + \Phi_2 P \log P \quad (15)$$

Here G and P are a free parameters related to the concentration of gelbstoff/detrital absorption and phytoplankton, respectively. The spectrally-dependent coefficients Φ_1 and Φ_2 are calculated from measurements as referenced in Lee et al. (1998). The physical quantity of Chlorophyll-a in units of mg m^{-3} is:

$$\text{Chl-a} = e^{(\log(P/0.06)/0.65)} \quad (16)$$

As a result of these models, the entire retrieval reproduces the spectral observation using just four free parameters: the glint Q , the backscatter X , the gelbstoff/detritus absorption G , and the phytoplankton absorption P . Each of these parameters can vary over the $[0, \infty)$ interval, so we treat the optimization as an unconstrained minimization of the logarithm of the free parameters. We use the Levenberg-Maquardt algorithm (More, 1978) to optimize the Sum Squared Error (SSE) fit between the model R_{rs} spectrum and the PRISM observation.

We validated the spectroscopic Chlorophyll-a algorithm using an observation by the PRISM ER-2 aircraft over Santa Monica Bay, coincident with a Landsat overpass and in-situ data collection. At the time of this flight, there was an algal bloom in progress due to a transient discharge from activities on shore. Figure 2 compares the standard multiband OC3 algorithm against the result of the full spectroscopic retrieval. The leftmost panel shows the entire flightline.

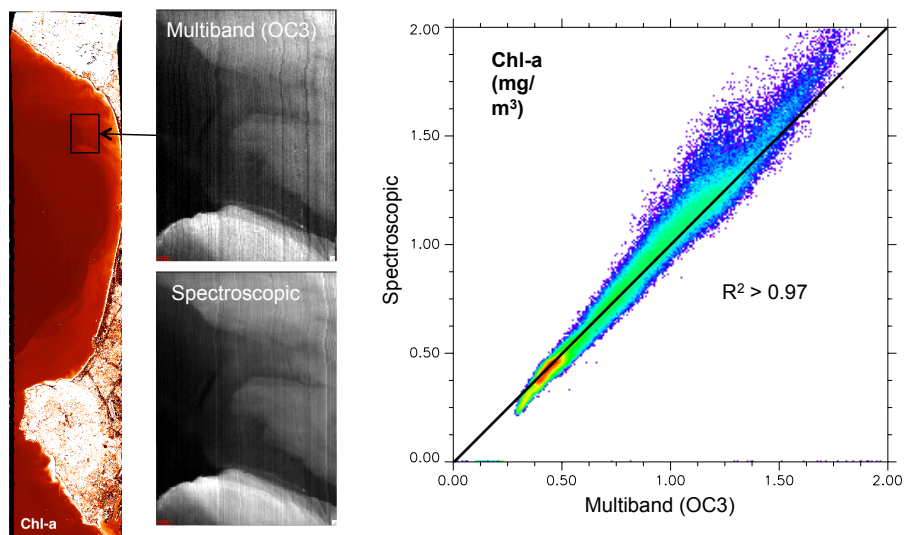


Figure 4: Comparison of in-situ Chl-a remote Chl-a retrievals using multiband (MODIS OC3) and spectroscopic algorithms.

Here the intensity of the image pixels correspond to the abundance of Chl-a. An insert shows a zoomed-in image of a high-contrast plume of phytoplankton. Here both algorithms identify very similar features, though the spectroscopic result is qualitatively smoother and more detailed. Values range from nearly 2 mg m^{-3} in the bright plume center to $<0.5 \text{ mg m}^{-3}$ in the dark areas. The scatter plot at right compares the two retrieved quantities directly. This reveals a very high R^2 value of greater than 0.97. The algorithms appear to diverge slightly at highest abundances, i.e. concentrations greater than 1.0 mg/m^3 . Despite these small differences, the comparison provides confidence that the two methods are consistent. The retrieved values are also consistent with Landsat images acquired of the same area.

3. Acknowledgements

A portion of the research described in this paper was performed by the Jet Propulsion laboratory, California Institute of Technology, under a contract with the National Aeronautics and Space Administration. Copyright 2015 California Institute of Technology. US Government Support Acknowledged.

4. Bibliography

Bruegge, C. J., Conel, J. E., Margolis, J. S., Green, R. O., Toon, G. C., Carrere, V., Holm, R. G., & Hoover, G. (1990). In-situ atmospheric water-vapor retrieval in support of aviris validation. *Imaging spectroscopy of the terrestrial environment*, (pp. 150–163).

- Dudhia, A. (2014). Oxford university reference forward model (rfm). <http://www.atm.ox.ac.uk/RFM/>, .
- Gao, B. C., & Goetz, A. F. (1990). Column atmospheric water vapor and vegetation liquid water retrievals from airborne imaging spectrometer data. *Journal of Geophysical Research: Atmospheres*, *95*, 3549–3564.
- Gao, B. C., Heidebrecht, K. B., & Goetz, A. F. (1993). Derivation of scaled surface reflectances from AVIRIS data. *Remote Sensing of Environment*, *44*, 165–178.
- Green, R. O., Eastwood, M. L., Sarture, C. M., Chrien, T. G., Aronsson, M., Chippendale, B. J., Faust, J. A., Pavri, B. E., Chovit, C. J., Solis, M. et al. (1998). Imaging spectroscopy and the airborne visible/infrared imaging spectrometer (aviris). *Remote Sensing of Environment*, *65*, 227–248.
- Johnson, R., Strutton, P. G., Wright, S. W., McMinn, A., & Meiners, K. M. (2013). Three improved satellite chlorophyll algorithms for the southern ocean. *Journal of Geophysical Research: Oceans*, *118*, 3694–3703. URL: <http://dx.doi.org/10.1002/jgrc.20270>. doi:10.1002/jgrc.20270.
- Lee, Z., Carder, K. L., & Du, K. (2004). Effects of molecular and particle scatterings on the model parameter for remote-sensing reflectance. *Applied Optics*, *43*, 4957–4964.
- Lee, Z., Carder, K. L., Mobley, C. D., Steward, R. G., & Patch, J. S. (1998). Hyperspectral remote sensing for shallow waters. i. a semianalytical model. *Applied Optics*, *37*, 6329–6338.
- Moline, M. A., Prezelin, B. B., & Schofield, O. (1997). Palmer lter: Stable interannual successional patterns of phytoplankton communities in the coastal waters off palmer station, antarctica. *Antarctic Journal of the United States*, *32*, 151.
- More, J. J. (1978). The levenberg-xmarquardt algorithm: implementation and theory. *Numerical analysis*, (pp. 105–116).
- Morel, A. (1974). Optical properties of pure water and pure sea water. *Optical Aspects of Oceanography*, (pp. 1–24).
- O'Reilly, J. E., Maritorena, S., Siegel, D. A., O'Brien, M. C., Toole, D., Mitchell, B. G., Kahru, M., Chavez, F. P., Strutton, P., Cota, G. F. et al. (2000). Ocean color chlorophyll a algorithms for seawifs, oc2, and oc4: Version 4. *SeaWiFS postlaunch calibration and validation analyses, Part, 3*, 9–23.
- PRISM (2015). *PRISM web site*, . URL: <http://prism.jpl.nasa.gov>.
- Rothman, L. S., Gordon, I. E., Babikov, Y., Barbe, A., Chris Benner, D., Bernath, P. F., Birk, M., Bizzocchi, L., Boudon, V., Brown, L. R. et al. (2013). The hitran2012 molecular spectroscopic database. *Journal of Quantitative Spectroscopy and Radiative Transfer*, *130*, 4–50.

- Schaepman-Strub, G., Schaepman, M. E., Painter, T. H., Dangel, S., & Martonchik, J. V. (2006). Reflectance quantities in optical remote sensing definitions and case studies. *Remote sensing of environment*, *103*, 27–42.
- Tanré, D., Deroo, C., Duhaut, P., Herman, M., Morcrette, J. J., Perbos, J., & Deschamps, P. Y. (1990). Technical note description of a computer code to simulate the satellite signal in the solar spectrum: the 5s code. *International Journal of Remote Sensing*, *11*, 659–668.
- Teillet, P. M. (1989). Surface reflectance retrieval using atmospheric correction algorithms. *Geoscience and Remote Sensing Symposium, IGARSS'89. 12th Canadian Symposium on Remote Sensing*, *2*, 864–867.
- Thompson, D. R., Gao, B.-C., Green, R. O., Roberts, D. A., Dennison, P. E., & Lundeen, S. R. (2015a). Atmospheric correction for global mapping spectroscopy: {ATREM} advances for the hyspirc preparatory campaign. *Remote Sensing of Environment*, *167*, 64 – 77.
- Thompson, D. R., Seidel, F. C., Gao, B. C., Gierach, M. M., Green, R. O., Kudela, R. M., & Mouroulis, P. (2015b). Optimizing irradiance estimates for coastal and inland water imaging spectroscopy. *Geophysical Research Letters*, *42*, 4116–4123. URL: <http://dx.doi.org/10.1002/2015GL063287>. doi:10.1002/2015GL063287.
- Vermote, E. F., Tanré, D., Deuze, J. L., Herman, M., & Morcrette, J. J. (1997). Second simulation of the satellite signal in the solar spectrum, 6s: An overview. *Geoscience and Remote Sensing, IEEE Transactions on*, *35*, 675–686.